Universiteit
Leiden
The Netherlands

Fundamental research on the voltammetry of polycrystalline gold

Yang, S.

Citation
Yang, S. (2024, April 9). *Fundamental research on the voltammetry of polycrystalline gold*. Retrieved from https://hdl.handle.net/1887/3731809

Version:	Publisher's Version
License:	Licence agreement concerning inclusion of doctoral thesis in the Institutional Repository of the University of Leiden
Downloaded from:	https://hdl.handle.net/1887/3731809

Note: To cite this publication please use the final published version (if applicable).

现在是过去的未来，
Now is the future of the past,
也是未来的过去。
also the past of the future.
Voltammetry

1

Introduction

1.1 Voltammetry as the central technique in electrochemical analysis

Over the past century, the field of electroanalysis has experienced a remarkable evolution, with voltammetry emerging as its central technique. Voltammetry is an electrochemical technique that involves applying a potential that varies with time to a working electrode and measuring the resulting current flowing between the working and counter electrodes. (Fig.1)

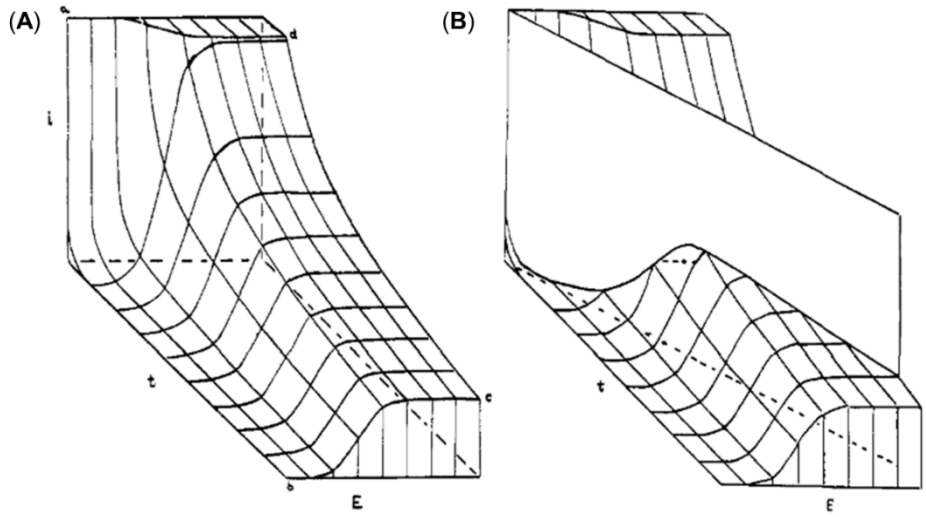

Fig. 1 The three-dimensional i-t-E surface for a Nernstian reaction. (**A**) The steady-state voltammogram corresponds to a cut parallel to the i-E plane. (**B**) another cut representing a linear potential sweep across this surface. Adapted from Reference [1].

In a relatively short period of just over 60 years, a diverse array of methods has been developed around voltammetry, specialized instruments have been designed and built, and a comprehensive theoretical and mathematical framework has been established.[2, 3] Since then voltammetry has become an essential technique in our current scientific research. It provides valuable information about the electrochemical properties and behavior of materials, which can have significant implications in fields such as materials science,[4-6] energy storage,[7-9] corrosion studies,[10-12] and sensor development.[13, 14]

A few specific examples of the importance of voltammetry on solid electrodes are given below:

(1). Electrode characterization

Voltammetry enables the determination of electrochemical parameters of the electrode materials, such as the electroactive surface area, charge transfer kinetics, and electrochemical stability.[15-17] These parameters are crucial for understanding the performance and behavior of electrodes in various applications.

(2). Material analysis

Voltammetry allows for the investigation of material properties and composition.[4-6] By studying the electrochemical behavior of an electrode, researchers can gain insights into the oxidation/reduction processes, interfacial reactions, and the surface reactivity of the material. This information is valuable for designing and optimizing electrode materials for energy storage devices such as batteries and supercapacitors.[9]

(3). Sensor development

Solid electrodes are often used in the development of electrochemical sensors. Voltammetry allows for the sensitive detection and quantification of analytes in various samples. By applying a potential to the electrode and measuring the resulting current response, it is possible to obtain information about the concentration, presence, or behavior of target analytes. This has applications in environmental monitoring, biomedical diagnostics, and industrial process control.[18]

(4). Corrosion studies

Voltammetry is used to study corrosion processes on electrode surfaces.[10-12] By monitoring the current response at different potentials, researchers can gain insights into the corrosion mechanisms, corrosion rates, and protective properties of coatings or inhibitors. This knowledge helps in the development of effective corrosion prevention strategies and the design of more corrosion-resistant materials.

(5). Energy conversion and storage

Solid electrodes play a crucial role in energy conversion and storage devices such as fuel cells, electrolyzes, and batteries.[7-9] Voltammetry allows for the investigation of electrochemical

reactions, charge/discharge processes, and performance characteristics of these electrodes, and thereby for the improvement of the efficiency, stability, and lifespan of energy storage systems.

In summary, voltammetry now becomes an indispensable tool for studying the electrochemical properties of materials, analyzing their behavior, and designing advanced technologies. It provides valuable information for materials characterization, sensor development, corrosion studies, and energy-related applications.

1.2 The history of Polarography — the forerunner of solid electrode voltammetry

Voltammetry originated in early 1922 when Heyrovsky initiated the measurement of current flow and drop time as a function of the potential at a dropping mercury electrode (DME).[19] The measurement wherein current-voltage curves on the DME were obtained were referred to as polarography.

On February 10 1922, Jaroslav Heyrovsky integrated a mirror galvanometer, a highly sensitive instrument, into the circuit. Through meticulous point-to-point measurements, he achieved a significant milestone by obtaining the first polarogram (Fig. 2). A few years later, Heyrovsky collaborated with Masuro Skikata (Fig. 3A) to develop an innovative instrument for the automatic recording of Cyclic Voltammetry (CV) curves, known as polarography (Fig. 3B). This pioneering work marked the advent of the first automated recording by an analytical instrument, signifying the onset of a new era in instrumental analysis.[20, 21]

At the time, mercury was widely regarded as the optimal electrode material for polarography.[22] The Dropping Mercury Electrode (DME) offered an easily renewable and atomically smooth surface, effectively mitigating issues related to electrode passivation and fouling. In addition, due to its high overpotential for the evolution of hydrogen, mercury exhibited a broad potential window, extending to negative potentials as low as ─1.6 V vs. SCE.[23] This unique property made mercury the preferred material for the determination of electrochemically reducible analytes.

From the 1940s to the early 1960s, polarographic methods on mercury electrodes experienced a rapid growth along two parallel paths. On one side, numerous variations of the traditional dropping mercury electrode emerged, including the mercury streaming electrode, the

hanging drop mercury electrode, the static mercury drop electrode, the mercury film electrode, the mercury amalgam electrode, the mercury microelectrode, the chemically modified mercury electrode, the controlled growth mercury electrode, and the contractible mercury drop electrode.[24] These innovations expanded the versatility and applicability of mercury-based polarography. On the other side, various modifications to the basic polarographic method were developed, such as oscillopolarography, Kalousek's switcher, AC polarography, Tast polarography, normal pulse polarography, differential pulse polarography, square-wave voltammetry, cyclic voltammetry, anodic stripping voltammetry, adsorptive stripping voltammetry, convolution techniques, and elimination methods.[19, 24] These advancements aimed to enhance the sensitivity, selectivity, and speed of polarography experiments, especially in light of trace analysis. Due to the increasing awareness of the potential toxicity of mercury, the utilization of mercury in polarography gave rise to increasing concerns, particularly from the 1960s onward. As a result, the practice of polarography diminished. It is widely believed that the decline of polarography can be primarily attributed to the apprehension surrounding mercury toxicity.[22, 25] However, despite the limited use of these derived polarographic methods, they have played a vital role in providing invaluable insights and experiences that have contributed significantly to the advancement of the electrochemical methodology as a whole.

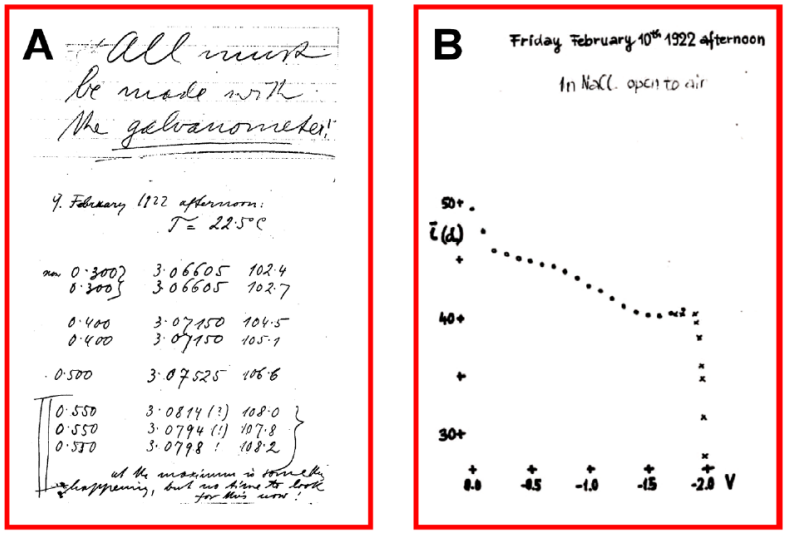

Fig.2 Image of two selected pages from Heyrovsky's laboratory notebook. Legend: (**A**) Protocol from February 9, 1922. On February 2, 1922, Heyrovsky conducted measurements of

electrocapillary curves in a 1 M NaCl solution exposed to air, but at the time did not realize what is going on at the maximum. (**B**) The first polarogram. Plot recorded on February 10, 1922. Adapted from Reference [22].

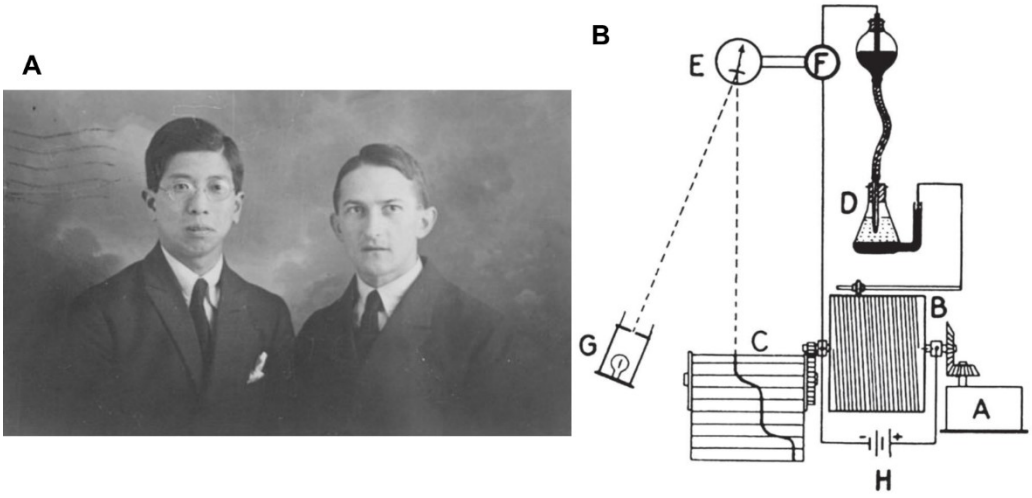

Fig.3 (**A**) Masuzo Shikata and Jaroslav Heyrovsky in London, December 12th 1923; (Adapted from Ref [19]). (**B**) Schematics of the Heyrovsky–Shikata photographic recording polarograph. Adapted from Reference [26].

1.3 The history of voltammetry on solid electrodes

The term "voltammetry" was officially adopted by the IUPAC Nomenclature Committee in the 1960s, but it was originally coined by Kolthoff and Laitinen in 1940 to describe voltage-controlled electrolytical methods.[27] Following this terminology, polarography was considered a specific form of voltammetry that utilized the Dropping Mercury Electrode (DME). When the mercury ceased to drop, the technique was no longer referred to as polarography, but rather as voltammetry with the Hanging Mercury Drop Electrode (HMDE). Since the 1960s, voltammetry techniques conducted at stationary and solid electrodes have gained popularity, gradually replacing the use of polarography with the DME.[2, 3]

The progress in voltammetry at solid electrodes was propelled by advancements in instrumentation.[2, 20] The use of operational amplifiers, initially based on vacuum tubes and later on transistors and integrated circuits, revolutionized the construction of electrochemical instruments.[20] In addition, the availability of Polaroid Land cameras and x-y recorders for

recording oscilloscope traces contributed to the field.[2] These developments facilitated the creation of more precise three-electrode static systems capable of accommodating various voltammetry modes such as lineal voltammetry, cyclic voltammetry, normal pulse voltammetry, differential pulse voltammetry, stripping voltammetry, etc.[28, 29] In addition, the advent of computers has had a profound impact on the advancement of instrumentation. In contemporary times, computer-controlled instrumentation is widely utilized, allowing for the implementation of various modifications of voltammetry using a single specialized apparatus.[2] Moreover, experiments can be automatically evaluated on a computer screen with the aid of suitable software that streamlines data analysis and enhances experimental efficiency.

Modern voltammetry techniques in combination with a rapid development of electrochemical instrumentation has largely encouraged electrochemists to step beyond trace metal determination and speciation, which had been the main application of polarography thus far, and to investigate more complex problems such as the corrosion of materials,[12, 30, 31] dissolution kinetics,[32, 33] structure-activity relationships of electrochemical processes,[34, 35] electrocatalysis,[36-38] kinetic studies of short-lived homogeneous reactions,[39, 40] and many other processes.

Since the 1960s, there has also been a growing research interest focused on the electrodes themselves. Electroanalytical chemists began delving into the physical chemistry of solid electrodes using voltammetry, and discussions aimed at designing and engineering modified electrodes emerged.[2] Initially, platinum, gold, and, to a lesser extent, silver were among the first solid electrodes studied as working electrodes.[12, 41] Subsequently, metals such as bismuth, nickel, palladium, rhodium, ruthenium, and indium, in various forms such as wires, plates, and disks, were also utilized for specific electroanalytical applications.[25] Following the initial surge of interest in solid noble metals, carbon-based electrodes gained rapid development due to their advantages such as a wider potential range, a more diverse surface chemistry, its chemical inertness, cost-effectiveness, and easy accessibility.[42-44] Simultaneously, in the mid-1970s, electrode modification techniques gained popularity with the aim of enhancing the sensitivity and selectivity of solid electrodes. Since then, various conductive materials have been explored for electrode modification purposes, including coatings composed of clays,[45] zeolites,[46]

inorganic crystals,[47] enzyme layers,[18] organic metals,[48] composites,[49] and nanomaterials.[50] These modified electrode materials have significantly advanced the development of various modern electrochemical sensors.

During the rapid development of voltammetry, significant discoveries have been made in electrochemical catalysts and energy storage materials. For instance, dimensionally stable anodes (DSA) were patented by Beer in the 1960s (in Britain) and 1970s (in the United States).[51] DSAs are coatings of a mixed ruthenium-titanium oxide (RTO), consisting of rutile RuO_2 and TiO_2 deposited on titanium. These coatings have found extensive use in industrial chlor-alkali and chlorate cells, leading to substantial energy savings due to their lower overpotentials at industrial current densities. The discovery of DSAs has been hailed as "one of the greatest technological breakthroughs of the past 50 years of electrochemistry".[52]

The first report on the nickel metal hydride battery (NiMH or Ni-MH) dates back to 1967.[53] In the 1970s, the advantage of using lithium metal for high-energy density storage systems was demonstrated through the assembly of primary lithium cells.[54, 55] During the same period, numerous inorganic compounds were found to react reversibly with alkali metals. These compounds, later identified as intercalation compounds, played a crucial role in the development of high-energy rechargeable lithium systems. The concept of electrochemical intercalation, fundamental to modern Li-ion batteries, was clearly defined in 1973.[56, 57]

Around the same time, the theoretical framework for pseudo-capacitance related to electrochemical supercapacitors was postulated by Conway and Gileadi.[58] Experimental observations revealed the rapid charge transfer processes of surface-bound species, such as underpotential deposition (UPD), adsorbed intermediates during electrolysis, and modified thin-film electrodes.[59] In 1971, Trasatti and his colleagues investigated the charge storage behavior of a ruthenium oxide thin film in sulfuric acid and discovered pseudo-capacitance in transition metal oxides for the first time. This discovery marked the beginning of research on electrochemical supercapacitor materials.[58, 60]

Overall, during this period, the thriving advancement of materials science across various fields has greatly ignited researchers' curiosity on the fundamental processes occurring at the solid-liquid interface.

1.4 The complexity and advantage of cyclic voltammetry on solid electrodes

In a conventional voltametric three-electrode setup, the electrode potential (E) is controlled between the working electrode (WE) and reference electrode (RE), while electrons flow between the counter electrode (CE) and the WE with the higher or lower electrochemical potential through the potentiostat, as depicted in Fig 4A. A voltammogram typically plots the resulting current (i) on the y-axis and the applied potential (E vs. the RE) on the x-axis. There are two primary processes depicted in the figures: one is the Faradaic process involving electron transfer (Fig. 4B) and the other is a non-Faradaic process without any electron transfer (Fig. 4C). In the absence of an electrochemical reaction, the electron flow cannot pass through the electrode-solution interface, resulting in a CV without any Faradaic current indicative of redox reactions (Fig. 4C). At a given potential, there will exist a charge on the metal electrode, q^M, and a charge in the solution, q^S. The charge on the metal, q^M, represents an excess or deficiency of electrons and resides in a very thin layer (0.1 Å) on the metal surface.[61, 62] The charge in solution, q^S , is made up of an excess of either cations or anions in the vicinity of the electrode surface. At all times, $q^M = - q^S$.[61] When E is scanned positively (the green line in Fig. 4B), the number of electrons decreases at the working electrode, resulting in a deficiency of electrons on the surface and a corresponding net positive surface charge. Conversely, when E is scanned negatively (the red line in Fig. 4B), the number of electrons increases, leading to an excess of electrons on the surface and a corresponding net negative surface charge. These positive or negative surface charges attract counterions to the electrode surface through electrostatic interactions. This process of physisorption is referred to as a non-Faradaic process, as illustrated in Fig. 4C.

In addition to non-Faradaic processes, there are also Faradaic processes that involve electron transfer between the working electrode and a reactant. Let us consider the electrochemical reaction of a species A from the solution, which has molecular orbitals (MO) including the highest occupied MO (HOMO) and the lowest unoccupied MO (LUMO). If the

Fermi level of the electrode is positioned higher than the HOMO but lower than the LUMO, no electron transfer occurs between the electrode and species A. However, by increasing E positively, a thermodynamic driving force is created, causing the energy level of metal electrons to gradually decrease until it becomes lower than the energy of the HOMO. At this point, a favorable condition is established for electrons to flow from species A to the electrode, resulting in the oxidation of species A ($A \rightarrow A^+ + e^-$). Conversely, if we decrease E negatively, the energy level of electrons gradually increases and becomes higher than the LUMO. In this scenario, electrons flow from the electrode to species A, leading to the reduction of species A ($A + e^- \rightarrow A^-$). The redox equilibrium of species A is described by the Nernst equation (eq 1). This equation establishes a relationship between the potential of an electrochemical cell (E), the standard potential of species A (E°), and the relative activities of the oxidized (Ox) and reduced (Red) forms of the analyte at equilibrium. The Nernst equation is expressed as follows:

$$E = E^{\circ} + \frac{RT}{nF} ln \frac{(Ox)}{(Red)} \quad (1)$$

Where R is the universal gas constant, T represents the temperature in Kelvin, n is the number of electrons involved in the redox reaction, and F is Faraday's constant.

To gain a better understanding of the relationship between the resulting current and the potential change in a cyclic voltammogram, let us consider the example of the reduction of ferrocenium (Fc^+) to ferrocene (Fc) (Fc=[Fe(Cp_2)]; Cp = cyclopentadienyl). Fig. 5H illustrates a typical cyclic voltammogram for a solution of Fc^+ undergoing a reversible one-electron reduction to Fc. The Nernst equation for the reaction $Fc^+ + e^- \rightleftharpoons Fc$ can be represented as follows:

$$E = E^{\circ} + \frac{RT}{nF} ln \frac{[Fc^+]}{[Fc]} \quad (2)$$

Changes in the applied potential at the electrode-liquid interface affect the equilibrium ratio of Fc+ and Fc, as determined by the Nernst equation. However, a different behavior emerges in the solution, where the Fc+:Fc ratio is governed by diffusion kinetics. Specifically, as the applied potential becomes sufficiently negative, the oxidized species (Fc+) present will undergo reduction at the electrode surface. This reduction leads to a diminishing concentration

of Fc^+ near the electrode, as illustrated in the concentration-distance profiles depicted in Fig. 5(A-G). This phenomenon is mirrored in the voltammogram by a peak in the current (i_p), succeeded by a decline in the current flow as the potential is further scanned negatively. Consequently, a concentration gradient is established, necessitating the transport of the oxidized species from the bulk solution to the electrode surface to enable additional current to flow.

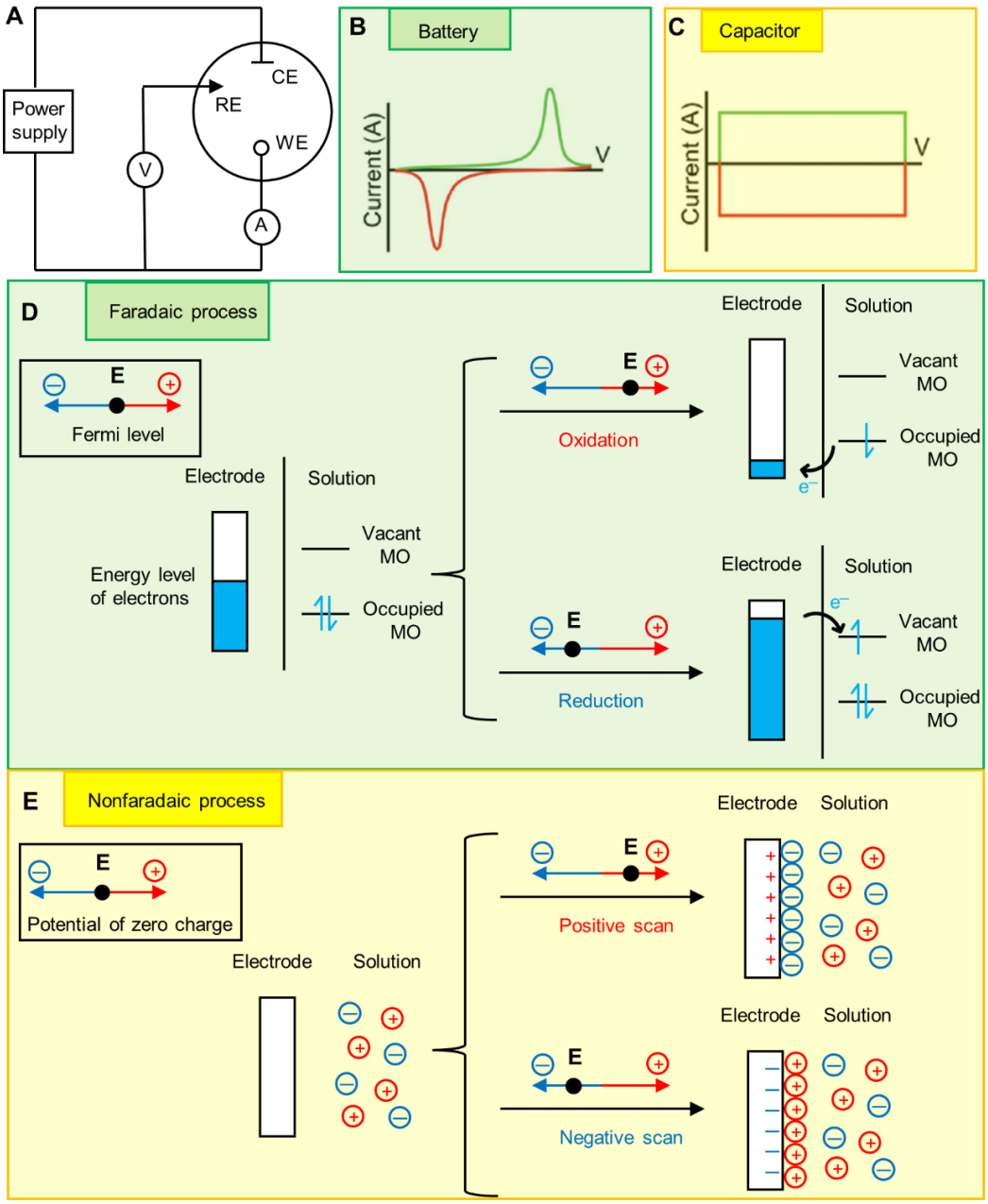

Fig.4 Cyclic voltammetry (CV) measurements. (**A**) Schematic of a typical three electrode electrochemical set up with the appropriate symbols used for Working Electrode (WE, O), Counter Electrode (CE, ⊥) and Reference Electrode (RE, arrow). (**B**) Representative CV illustrating electron transfer within a battery system. (**C**) Exemplary CV depicting for a physical capacitor behavior devoid of electron transfer. (**D**) Representation of Faradaic oxidation and reduction process of species (chemical processes with electrons transfer) in solutions with the change of applied potential of electrode. The molecular orbitals (MO) of species shown are the highest occupied MO and the lowest vacant MO. (**E**) Representation of a Non-faradaic process driven by electrostatic forces arising from extra positive and negative charges at the surface. B and C adapted from Reference [63].

In cyclic voltammetry, the speed of a redox reaction is governed by the sweep rate (ν, mV s^{-1}). Taking into account the difference in kinetic limitations, the current response to the sweep rate (ν) depends on whether the redox reaction is diffusion-controlled or surface-controlled.[64, 65] If a redox reaction is controlled by the semi-infinite diffusion process, the current response varies with $\nu^{1/2}$(eq 3) (Fig. 6A).[5, 64] Diffusion controlled redox reactions encompass a wide range homogeneous electrochemical catalytic processes, and voltammograms prove accurate kinetic information to investigating their kinetics.

$$I_{(V)} = a\nu^{1/2} \quad (3)$$

$$I_{(V)} = a\nu \quad (4)$$

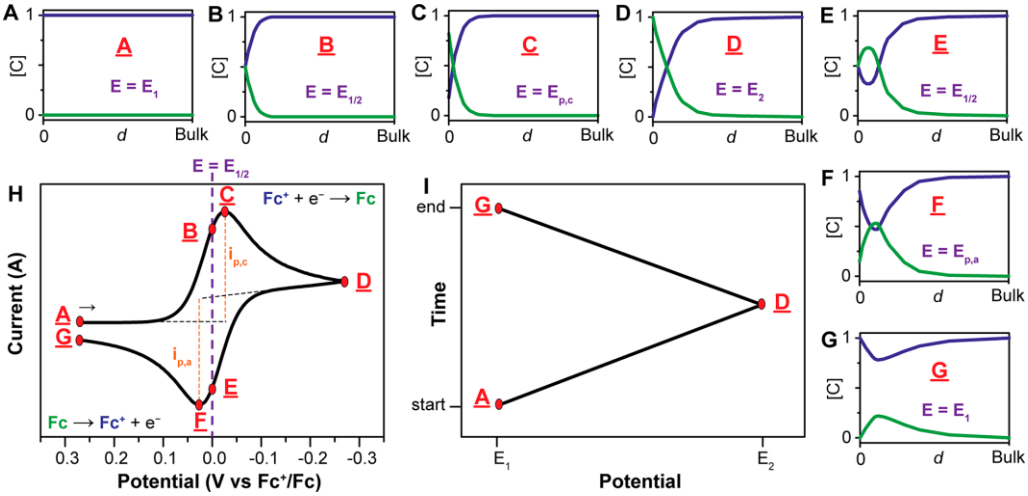

Fig. 5 (**A**–**G**): Concentration profiles (mM) for Fc^+ (blue) and Fc (green) as a function of the distance from the electrode (d, from the electrode surface to the bulk solution, e.g. 0.5 mm) at various points during the voltammogram. (**H**): Voltammogram of the reversible reduction of a 1 mM Fc^+ solution to Fc, at a scan rate of 100 mV s^{-1}. (**I**): Applied potential as a function of time for a generic cyclic voltammetry experiment, with the initial, switching, and end potentials represented (A, D, and G, respectively). Adapted from Reference [5].

If a redox reaction is limited by a surface reaction wherein diffusion does not play a role, the current would vary directly with ν (eq 4) (Fig. 6B).[64, 66] Such surface redox reactions are referred to as pseudocapacitance, which was introduced in the early 1960s to describe surface Faradaic process such as underpotential deposition and hydrogen adsorption.[58] It was later extended to energy storage in the early 1970s when researchers observed that thin films of hydrous RuO_2 cycled in an acidic electrolyte exhibited cyclic voltammograms resembling those of capacitors, while single-crystal RuO_2 did not exhibit such behavior.[60] Since then, more and more examples of pseudocapacitance behavior have been identified including (1) redox reactions (2), intercalation of cations (3), doping and de-doping in conductive polymers (4) and underpotential deposition of metals (Fig. 7).[63] Especially the discovery of surface redox reactions has opened up a new world of opportunities to enhance the specific capacitance of various energy storage systems.

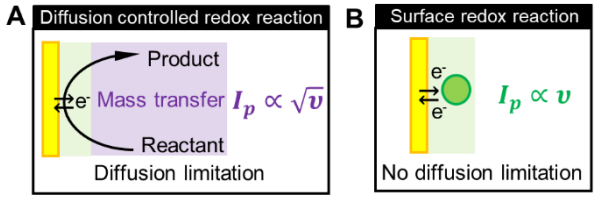

Fig. 6 (**A**) Schematic representation of a diffusion controlled redox reaction and its electrochemical response in which the peak current (I_p) varies with the square root of the scan rate ($\sqrt{v}$). (**B**) Schematic representation of surface redox reaction and its electrochemical response that shows the peak current (I_p) varies with the scan rate (v).

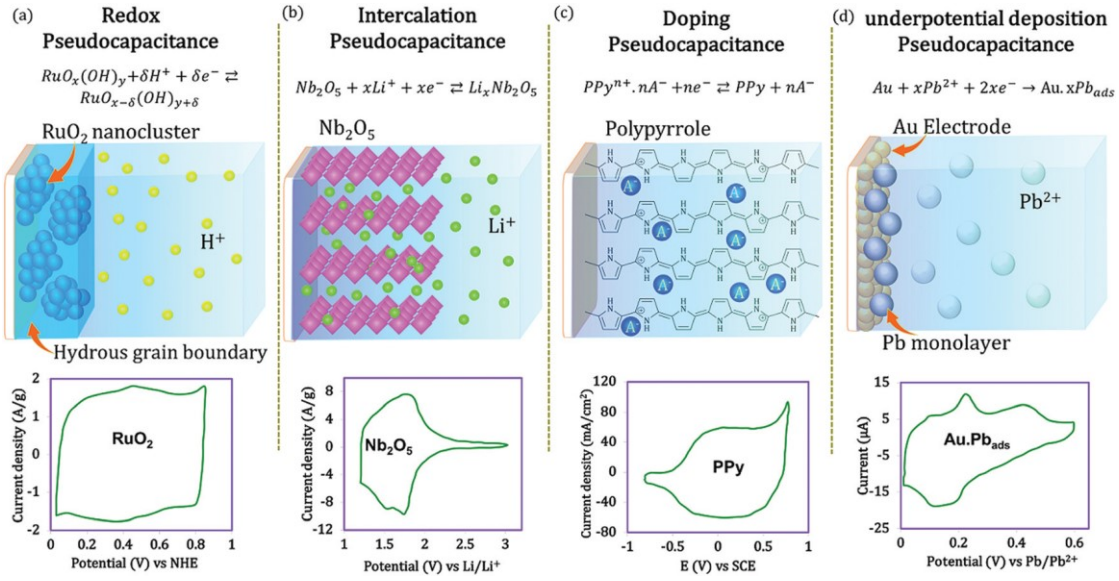

Fig.7 Different types of redox mechanisms that give rise to pseudocapacitance. (**a**) Redox pseudocapacitance, as in RuO_2•xH_2O. (**b**) Intercalation pseudocapacitance, as in Nb_2O_5. (**c**) Doping pseudocapacitance, as in polypyrrole and (**d**) underpotential deposition based pseudocapacitance, as in the deposition of lead on the surface of a gold electrode. Adapted from Reference [63].

The complexity of a redox reaction is also reflected in the electron transfer mechanism. For an electrochemical reaction, especially a multielectron reaction process, the reaction process involves various intermediates. Let us consider the oxygen reduction reaction (ORR) as an example. The ORR process involves different oxygenated intermediates, such as OH^-, HO_2^-, O_2^{2-} and O_2^-. On basis of whether oxygen directly adsorbs on the catalyst, the ORR process can be simply separated into a surface-dependent inner-sphere electron transfer mechanism and a surface-independent outer-sphere electron transfer mechanism.[67] In the inner-sphere reactions, O_2 binds to the electrode surface and the electrons are transferred directly from the material surface to the specifically adsorbed intermediates, as shown in Fig. 8a. In this case, the ORR kinetics are mainly governed by the binding energies between oxygenated intermediates and the catalyst.[68] In outer-sphere reactions, no chemisorption of oxygen takes place, and the ORR must involve electron tunneling across the solvent layer, which separates the oxygenated intermediates from the electrode surface, as shown in Fig. 8b. While numerous

in situ spectroscopic techniques can aid confirming the presence of intermediates, the question of whether these species remain in solution or undergo adsorption onto the electrode surface remains a subject of ongoing debate.[69]

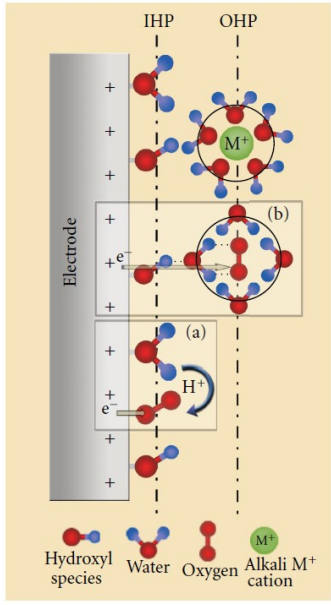

Fig. 8 Schematic illustration of the double-layer structure during the oxygen reduction reaction (ORR) in alkaline media. Insets illustrate inner-sphere (a) and outer-sphere (b) electron transfer processes. Adapted from Reference [70].

The complexity of voltammetry stems from the coexistence of various species at the electrode-solution interface, each exhibiting complex non-Faradaic and/or Faradaic processes. The measured E-I relationship in voltammetry represents a combination of all these processes, involving intricate theories. However, despite its complexity, voltammetry at solid electrodes has rapidly become one of the most widely used electrochemical methods, primarily due to significant advancements in the chemical analysis.[20] A key advantage of solid electrode voltammetry is its seamless integration with other techniques, facilitating the development of diverse in situ methods, such as steady-state mass transfer study at rotating electrodes,[71, 72] in situ spectroscopic methods,[73, 74] scanning electrochemical microscopy,[75] in situ mass spectrometry,[36] in situ quartz crystal microbalance techniques,[76, 77] in situ atomic force

microscopy,[78] et. al. These integrated approaches provide invaluable insights into the complex microscopic phenomena taking place at the electrode-interface.

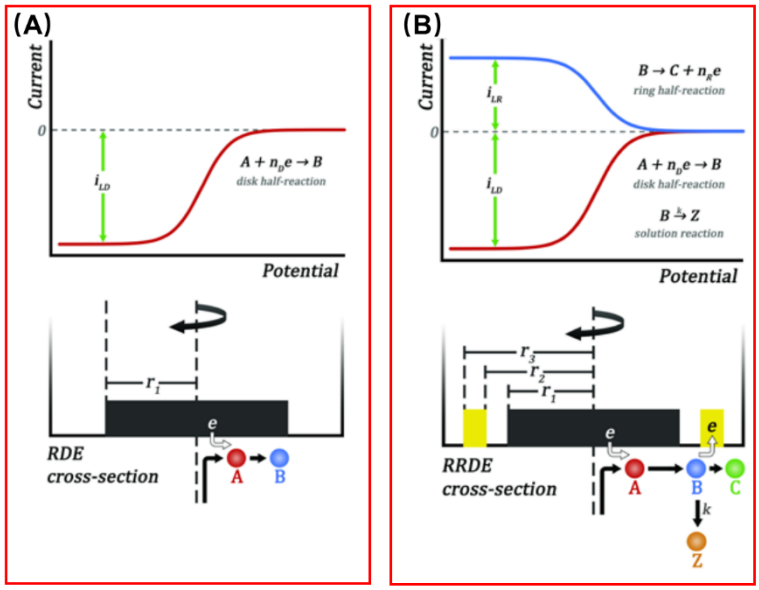

Fig. 9 (**A**) Steady-state mass transport at the Rotating Disk Electrode (RDE) conveys material from the bulk solution towards the disk. The Levich equation predicts the limiting current (i_{LD}) observed as species A is reduced to B. (**B**) Mass transport at the Rotating Ring-Disk Electrode (RRDE) first conveys species A from the bulk solution to the disk electrode where it is reduced to B. The species B is swept to the ring electrode and detected as an anodic current as it is oxidized to C. In some systems, as B transits from the disk to the ring, it may undergo a competing side reaction in solution, lowering the observed ring current. The RRDE may be used to probe the kinetics of such side reactions. Adapted from Reference [72].

One of the most important advances in solid electrode voltammetry is the investigation of the hydrodynamic behavior of a reaction at the interface by performing voltammetry with a rotating disk electrode (RDE). The RDE methodology was first introduced by Levich and his colleagues.[72] When the potential of the RDE is maintained at (or swept to) a sufficiently negative value, the cathodic current is limited solely by the rate of mass transport of species A to the disk surface in presence of a proficient catalyst (Fig. 9A). Under these conditions, an expression for the limiting current (i_{LD}), known as the Levich equation, can be written as follows:

$$i_{LD} = 0.62 n_D F (\pi r_1^2) C_A^* D_A^{2/3} \nu^{-1/6} \omega^{1/2} \quad (3)$$

Where F is the Faraday constant, r_1 is the radius of the disk electrode, C_A^* is the concentration of the electroactive species A in the bulk solution, D_A is the diffusion coefficient of the electroactive species, ν is the kinematic viscosity of the solution, and ω is the angular rotation rate of the disk electrode. Levich's development of the rotating disk electrode (RDE) was highly significant as it offered an experimentally reproducible and mathematically well-defined method for electrochemists to precisely control the rate at which an electroactive species reaches the electrode surface. This technique has been instrumental in advancing our understanding of mass transport phenomena and reaction kinetics at solid electrode interfaces.[79, 80]

Additional important hydrodynamic voltammetry technique involves using a rotating ring-disk electrode (RRDE), which is very similar to a RDE.[72] The main difference is that the RRDE includes a second working electrode in the form of a ring surrounding the central disk of the first working electrode. In the RRDE experiment, the convection-diffusion mass transport can carry a portion of the products generated at the disk electrode to the ring electrode, as illustrated in Fig. 9B. For instance, in the case of a species A being reduced to B at the disk electrode ($A + n_D e^- \rightarrow B$), the limiting cathodic current at the disk is given by the Levich equation (Eq. 3). An anodic half-reaction may be used to detect B as it arrives at the ring electrode ($B \rightarrow C + n_R e^-$). The anodic limiting current at the ring electrode (i_{LR}) can be expressed in terms of the cathodic limiting current at the disk electrode (i_{LD}) as follows:

$$i_{LR} = -i_{LD} (n_R / n_D) N_{max} \quad (4)$$

Where N_{max} is the maximum theoretical collection efficiency, which is a unitless value indicating the fraction of material from the disk that is theoretically expected to arrive at the ring.[40] This value of N_{max} is influenced by the geometric characteristics, such as the shape and size, of the ring and disk electrodes. As long as the electron transfer kinetics are suitably rapid and concentration-dependent, the collection efficiency is primarily governed by the geometric factors of the electrodes, regardless of the specific electrochemical reactions taking place. The key point is that N_{max} is determined solely by the physical dimensions of the electrodes and is

not influenced by the electrochemical processes themselves. The ring-disk geometry provides a distinctive approach to investigate the behavior of unstable catalytic intermediates, enabling in situ monitoring as a direct function of the applied reaction conditions.

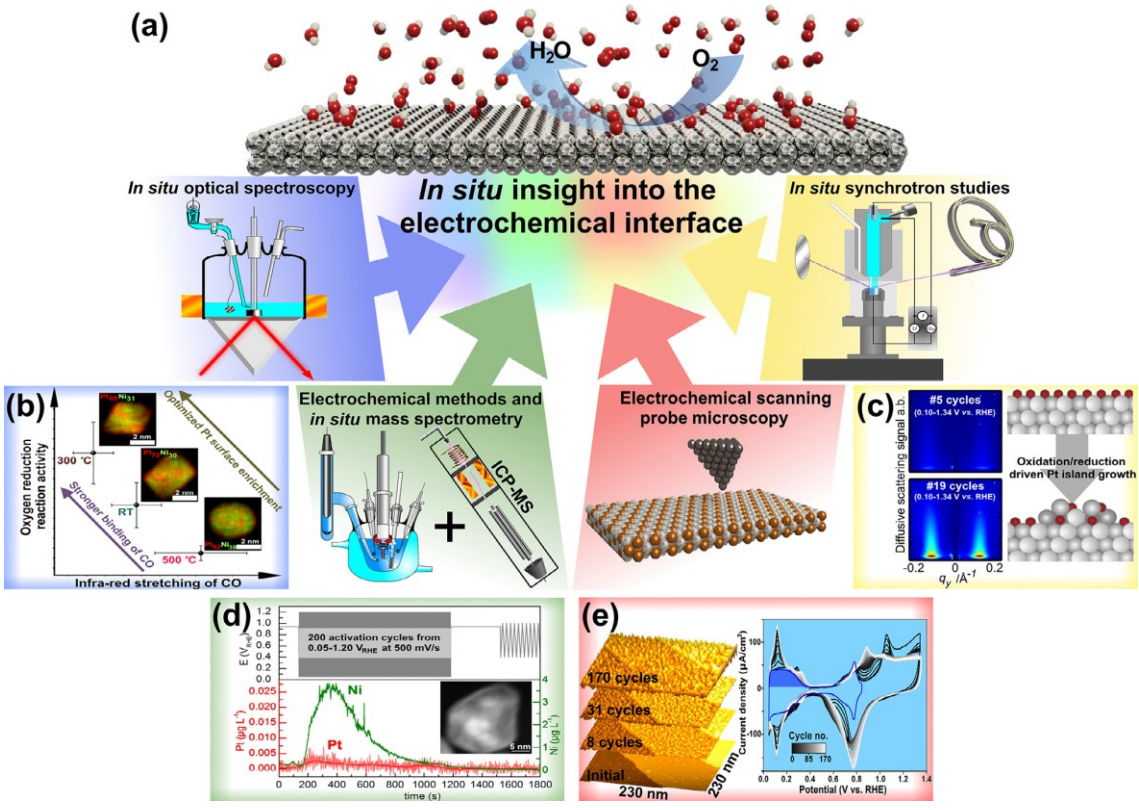

Fig. 10 Selection of in situ characterization of the electrochemical interface of relevance for the ORR: (**a**) Schematic representation of a selection of techniques that provide an in situ insight into ORR electrocatalysts: in situ optical spectroscopy, electrochemical methods combined with mass spectrometry, electrochemical scanning probe microscopy and in situ X-ray characterization techniques. (**b**) Correlation of CO stretching from in situ FTIR with the ORR activity of Pt-Ni nanoparticles. (**c**) Pt(111) oxidation and catalyst roughening probed by in situ GI-XRD. (**d**) Electrochemical flow cell combined with ICP-MS monitoring the Pt/Ni dissolution during dealloying of Pt-Ni nanoparticles. (**e**) In situ STM images and CVs of a Pt(111) electrode surface during oxidation-reduction cycles. Adapted from Reference [81].

Another important advantage of solid electrode voltammetry is the ability to trace formed intermediates of electrochemical reactions in situ and identify the active phase of catalysts at a

particular applied potential by combining it with various techniques. To date, there are numerous advanced in situ electrochemical characterization techniques that enable probing the electrode-interface at the atomic and molecular level, as depicted in Fig. 10. These techniques include in situ spectroscopy,[73, 74] in situ mass spectrometry,[36] scanning probe microscopy,[75, 78] in situ synchrotron studies,[81] and in situ quartz crystal microbalance (QCM).[76, 77] The integration of these in situ electrochemical techniques is pivotal in yielding valuable insights into the intricate relationships between a material's structure and its reactivity, as well as the underlying mechanisms of reactions.

In the context of this thesis, our focus will primarily be on elucidating the principles of the electrochemical quartz crystal microbalance (EQCM) to illustrate the seamless synergy between voltammetry and quartz crystal microbalance (QCM) technology. The potential usefulness of QCM as a mass sensor was first demonstrated by Sauerbrey in 1959. The technique relies on acoustic wave devices based on piezoelectric resonators whose frequency responses are related to the mass change per unit area at the QCM surface.[82] According to the Sauerbrey equation (Eq. 5), a mass change (Δm) at the surface induces a shift in the resonance frequency (Δf) of the QCM, enabling the detection of sub-monolayer weight changes, as illustrated in the Fig. 11.[83]

$$\Delta m = -C_m \Delta f \quad (5)$$

Where C_m is the proportionality constant that depends only on the properties and dimensions of the quartz crystal resonator.

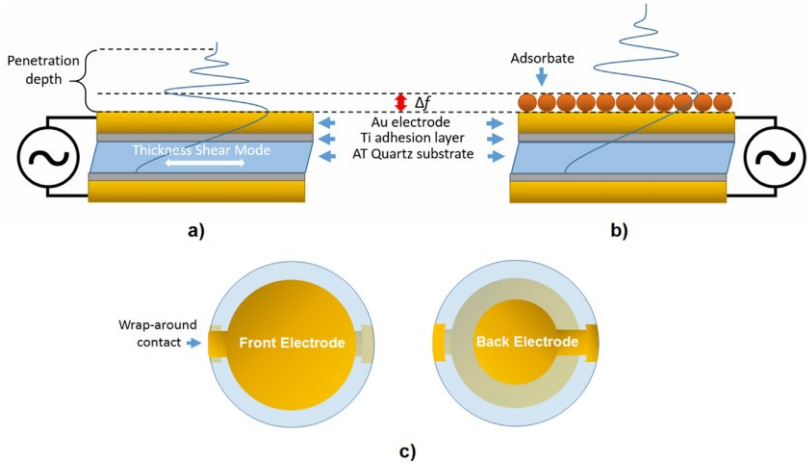

Fig. 11 Schematic cross-section of a quartz crystal showing thickness sheer oscillation overlaid with the fundamental resonance wave (**a**), the change in oscillation resonance frequency ($\triangle f$) when a rigid mass adsorbs to the surface (**b**) and front and back view of a quartz crystal with wrap-around electrode typically used for liquid measurements (**c**). Adapted from Reference [83].

The applicability of the QCM was extended to liquid based systems by Nomura and Okuhara in their publication in 1982, sparking the development of the EQCM for the field of interfacial electrochemistry.[84] Initially, QCMs were mainly used as thin film deposition monitors to control the film thickness. However the combination of electrochemistry and QCM operation has opened up new insights into interfacial electrochemical processes.[85, 86]

For a long time, directly uncovering whether a reaction process is homogenous or heterogenous has been a challenge.[39, 85] Although spectroscopic evidence can confirm the existence of different types of intermediates at the electrode interface, it remained unclear whether the formed intermediates remained in solution or in an adsorbed state on the catalyst.[69] The EQCM technique allows for the in situ measurement of mass changes occurring at the electrode as the applied potential is scanned during a CV experiment. For a homogenous reaction process, the mass response shows no significant change during different CV cycles, whereas an experiment in which a heterogeneous deposit is formed, the mass response shows a significant increase with the number of CV cycles or time in an amperometry experiment, as shown in Fig. 12. This capability of EQCM offers valuable information to distinguish between homogeneous and heterogeneous electrochemical processes at the electrode interface. However, for an extended period, any alteration in the oscillation resonance frequency of EQCM was often simplistically attributed solely to electrochemical deposition on the surface.[87] Nevertheless, numerous researchers have discovered that the calculated mass change derived from frequency changes can exceed the theoretically expected maximum amount of electrochemical deposition in electrolyte solutions,[76, 88] The underlying reasons for this phenomenon are believed to be associated with variations in solution viscosity and density resulting from shifts in the applied potential.[89] The precise quantification of these effects remains elusive, consequently constraining the accuracy of EQCM measurements.

While measuring potential (E) and current (I) might seem straightforward, confirming the precise factors responsible for the alterations in the E-I relationship in voltammetry is challenging. Fortunately, the development of in situ electrochemical methods has allowed us to gradually unveil the rich and mysterious information hidden within the voltammogram. These advanced techniques provide valuable insights into the intricate processes occurring at the electrode-interface, shedding light on the underlying mechanisms and revealing the intricate dynamics of electrochemical reactions. As a result, the voltammetry technique has become even more powerful and informative, playing a pivotal role in advancing our understanding of electrochemical processes and catalysis in various applications.

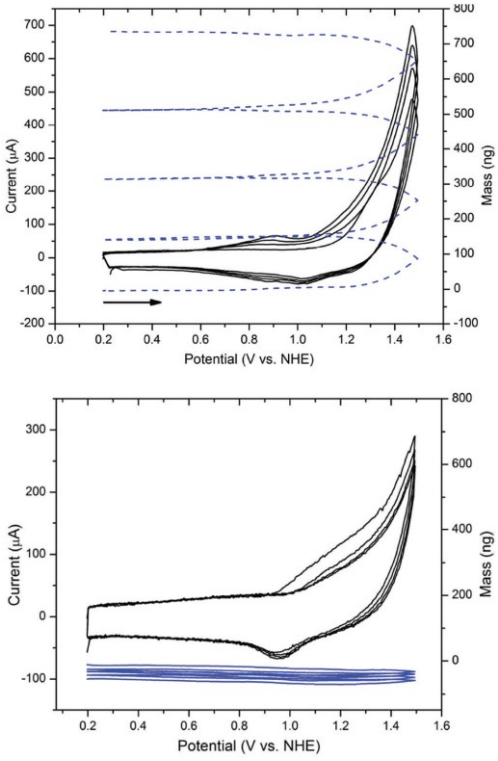

Fig. 12 Difference in the EQCM response of a deposition formed from the precursor $[Ir(Cp^*)(OH_2)_3]SO_4$ (top) and formation of a homogeneous catalyst from the precursor $[Ir(Cp^*)(pyalc)(CF_3COO)]$ (bottom).† The currents are depicted in black and the mass trace in blue. Cp*=pentamethylcyclopentadienyl; pyalc = 2-(2′-pyridyl)-2-propanolate. Adapted from Reference [85].

1.5 Remaining challenges in Voltammetry

Although the progress of in situ techniques has certainly enriched our comprehension of electrochemical processes, the fundamental challenges of understanding Faradaic and non-Faradaic currents in voltammetry persist within the broader context of energy convection systems. This thesis will concentrate on addressing the two most important fundamental questions in the realm of voltammetry.

The question one: *What is the relation between the applied potential and the surface charge, and the structure of both the surface and surface-liquid interface?*

The relation between the applied potential and surface charge

In an electrochemical reaction, the electrode potential serves as the driving force for the electrochemical process.[62] As the net surface excess charge changes through the potentiostat during positive or negative scanning of the potential, the electrochemical potential of the electrons on the working electrode either increase or decrease accordingly. The change in potential leads to a redistribution of ions, resulting in the formation of an electric double layer (EDL) at the interface between the electrode and the surrounding solution.[61] The EDL formation is an example of a non-Faradaic process, as shown in Fig. 4C.

A crucial concept in understanding the excess charge and potential effects at the electrode interface is the potential of zero charge (PZC). The PZC is defined as the potential at which no net excess charge exists on the electrode surface, but it is essential to recognize that the PZC is significantly influenced by the surface characteristics and material properties of the electrode.[90-92] Initial insights into the concept of excess charge and the PZC were obtained from measurements of the surface tension at mercury-electrolyte interfaces, as depicted in Fig. 13A.[93] In these surface tension measurements, the liquid mercury electrode provides a clean and well-defined surface structure, and a wide potential range where only non-Faradaic processes occur. The PZC is identified as the potential at which the surface tension is maximal (Fig. 13B).[93] However, conducting such surface tension measurement is not feasible at solid materials.

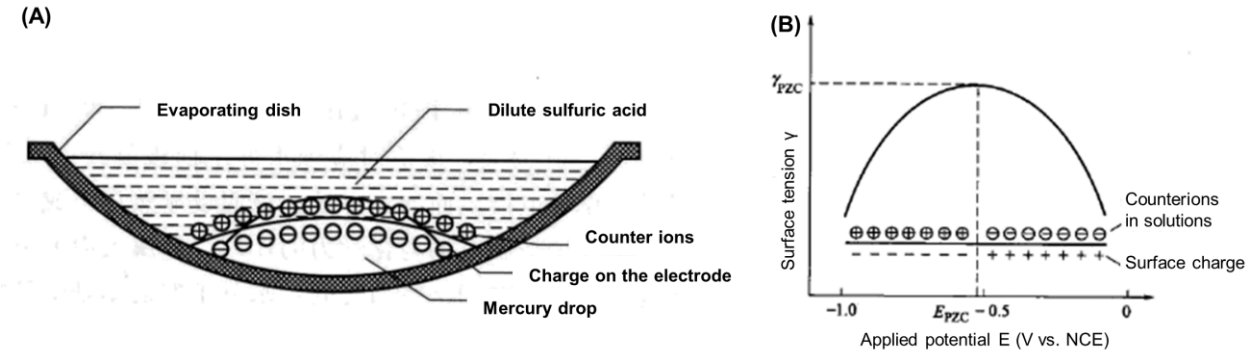

Fig. 13 (**A**) The surface leveling phenomenon when a double layer is formed on the surface of a mercury drop. The figure illustrates the scenario with a negatively charged surface. (**B**) Electrocapillary curve of the dropping mercury electrode (DME), where E_{PZC} is the potential of zero charge, and γ_{PZC} is the surface tension at the E_{PZC}. Adapted from Reference [94].

Variations in the surface excess charge will induce a redistribution of ions, resulting in the non-Faradaic currents that can be observed in a CV. Electrochemical capacitance measurements calculated from the current responses in a voltammogram have played a crucial role in understanding the electrochemical interface structure on the electrode surface, particularly for solid electrodes. For example, in a voltammetry measurement, a differential capacitance (C) is determined using the following equation:

$$C = \frac{I}{\nu \times S} \quad (6)$$

where I is the current (A), ν is the scan rate (V/s) and S is the electrode surface (m^2). Based on the research of the differential capacitance, the classical model for EDL known as the Gouy-Chapman-Stern (GCS) model was developed and show in Fig. 14.[95, 96] In the GCS model, the total capacitance of the electric double layer (C_{GCS}) can be divided into two components: the inner layer or Helmholz capacitance (C_H) and the diffuse layer or Gouy-Chapman capacitance (C_{GC}):

$$\frac{1}{C_{GCS}} = \frac{1}{C_H} + \frac{1}{C_{GC}} \quad (7)$$

In a measurement to determine the non-Faradaic current, there is a key premise that the current observed in the voltammogram should be entirely attributed to non-Faradaic currents.

Non-Faradaic currents are electrostatic in nature and result from the adsorption or desorption of ions from the electrolyte solution onto the electrode surface without any involvement of electron transfer processes.

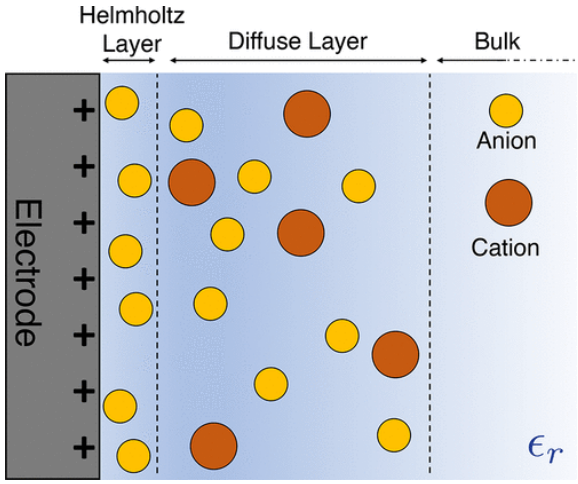

Fig. 14 Schematic representation of the electrical double layer at a planar electrode according to the GCS model. Anions are displayed in yellow, and cations are in orange. They are immersed in a dielectric continuum of relative permittivity ϵ_r. Adapted from Reference [96].

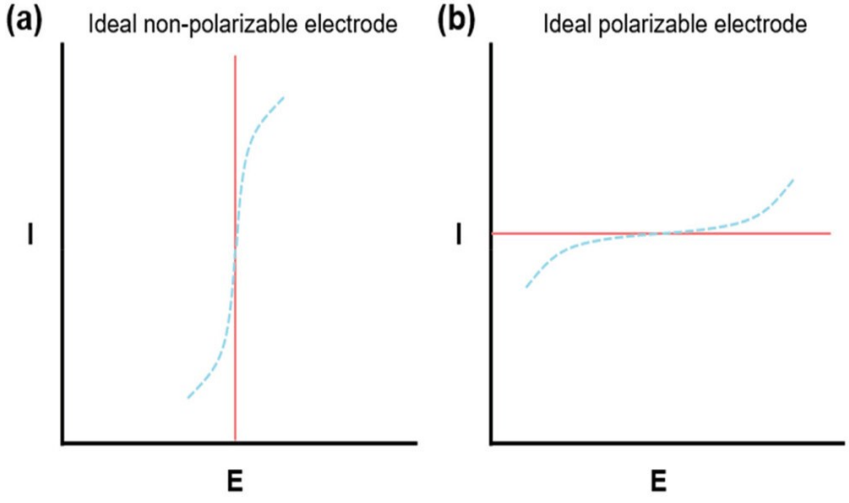

Fig. 15 Polarization behaviors of (**a**) an ideal non-polarizable electrode and (**b**) an ideal polarizable electrode (red lines). Blue dotted lines indicate that the practical electrode deviates from the ideal situation beyond a certain current or potential range. Adapted from Reference [97].

Polarization is defined as "*the divergence of the electrode (or cell) potential (E) from its equilibrium value (E_{eq}) for a cell or electrode possessing a distinct equilibrium potential*" , according to the dictionary of electrochemistry.[98] In the context of voltammetry, the process can be considered as a potentiostatic polarization, i.e. driven by the potentiostat. Fig. 4B and C illustrates two ideal current responses that an electrode may have when the applied potential is changed.

An electrode that exhibits no charge transfer across the electrode-solution interface during polarization is referred to as an ideal polarized electrode (as indicated in the red line of the Fig. 15b). Its behavior is analogous to that of a capacitor (Fig. 4C). Under this scenario, where the capacitance remains constant, the current response maintains constant, resulting in the manifestation of a rectangular shape of the CV, governed by the relationship wherein the current is directly proportional to the scan rate (Eq. 8).

$$I = C \times \nu \quad (8)$$

Moreover, a consistent current flows until a sufficient amount of charge (q) has accumulated to be balanced on the charge of the electrode surface, following the equation (Eq. 9).

$$\frac{\mathrm{d}q}{\mathrm{d}E} = C \quad (9)$$

In reality, a solid electrode is more complex, both in terms of physical and chemical characteristics of the electrode surface, including the crystallographic orientation, surface defects, surface roughness, the presence of adsorbed species, and any modifications or coatings.[61, 99] When the potential changes, various chemical processes, including electron transfer from the electrode structure to electrolytes and solvents in the solutions, can alter the current response in the potential region of polarization.

The concept of an ideal non-polarized electrode is therefore a hypothetical one, representing an electrode where a Faradaic current can flow freely without any change in potential from its equilibrium value. In this scenario, where there is no diffusion, the electrode reaction is considered to be infinitely fast, resulting in an infinite current density (as indicated

in the red line of the Fig. 15a). However, this ideal situation is not achievable in reality. When the potential continues to change, the surface concentration of the reactant must decrease, leading to an decreased flux of electrons towards the surface. Eventually, depletion effects of reactant come into play, and an infinite current response for an ideal non-polarization process becomes impossible. In practical terms, no electrode can be truly non-polarizable, as there will always be some limitations and factors that influence the electrochemical processes at the electrode-solution interface. The actual behavior of a solid electrode lies somewhere between the ideal polarized and ideal non-polarizable scenarios (as indicated by the blue dots in the Fig. 15).[97]

One of the challenges in electrochemical measurements is the difficulty of separating the non-Faradaic current arising from the electric double layer (EDL) from the Faradaic current caused by reactions that involve charge transfer. When a redox reaction occurs, the resulting Faradaic currents will be entangled with the non-Faradaic current of the EDL. As a result, it becomes challenging to precisely determine the exact potential of zero charge (PZC) and how the excess charge that has accumulated on the electrode surface changes, as the real EDL capacitance is unknown. Over time, researchers have developed more complex physicochemical models by considering various factors in addition to the classical Gouy-Chapman-Stern (GCS) model.[96] These factors include the field-dependent orientation of water molecules, the discreteness of adsorbed ions, and quantum effects of metal electrons.[61, 95, 100] However, attempts to obtain perfect or even satisfactory fits of the capacitance by adjusting multiple factors can easily lead to overfitting, if the model becomes too complex, and thereby loses any predictive accuracy in the process. To allow for sufficient experimental data to calibrate these models on, it is essential to perform precise experiments that directly trace the change of the excess charge on the electrode surface without being influenced by chemisorption or chemical reactions.

Discovering novel in situ techniques or exploring the potential applications of existing in situ methods that allow for the direct observation and measurement of changes in the excess charge on the electrode surface, that is separated from any current contributions from chemisorption processes or redox reactions, is of utmost importance. Such methodologies

would provide valuable insights into the intricate question "*What is the relation between the applied potential and surface charge?*" Accordingly, this thesis tackles precisely such an exploration of existing methods. These advancements would significantly enhance our understanding of complex electrochemical processes and pave the way for more accurate modeling and interpretation of electrochemical data.

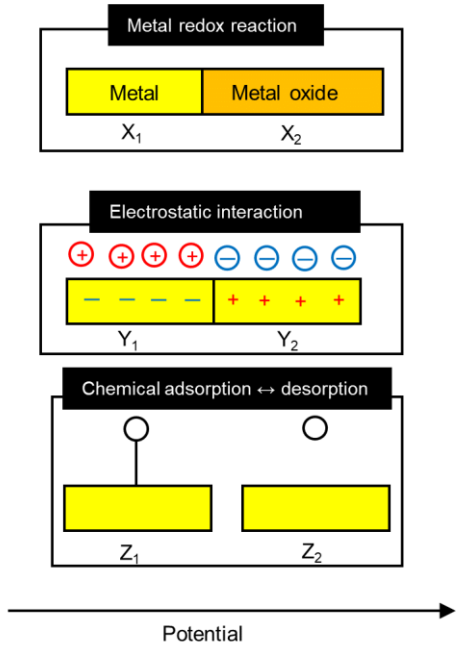

Fig. 16 Schematic representation illustrating three potential electrochemical processes occurring when the potential changes on a metal electrode. X_1 and X_2 depict alterations in the electrode surface between metal and metal oxide with changes in the applied potential. Y_1 and Y_2 correspond to positive and negative excess charges, respectively, attracting counterions electrostatically. Z_1 and Z_2 signify the chemical adsorption and desorption process of ions, respectively.

The structure of the surface and surface-liquid interface

The difficulties in comprehending the solid-liquid interface structure, where the solid electrode interfaces with the solution, arise not only from the interplay between Faradaic and non-Faradaic currents but also from the structural alterations occurring on the electrode due to

the presence of chemisorbed electrolytes, solvents, and even concurrent corrosion or passivation processes.[35, 101, 102] All these processes are influenced by changes in potential.

In a voltammogram, a solid electrode can undergo oxidation and reduction processes, resulting in different regions based on the metal region (X_1) and metal oxide region (X_2), as depicted in Fig. 16. Within both the metal region and the metal oxide region, there coexist different electrostatic interactions (represented as Y_1 and Y_2) and various chemical adsorption and desorption phenomena (represented as Z_1 and Z_2). Concerning the interface structure at the metal region (X_1), a significant challenge arises in quantification of the ion distribution at the solid – liquid interface. This task is complicated by the difficulty of discerning between non-Faradaic and Faradaic currents in CVs. To address this, the key lies in discovering a direct analytical method capable of identifying the surface charge density, which plays a direct role in governing the ion distribution at the interface.

In the realm of the interface structure, another challenge is the accurate identification of the oxide structure in the oxide region (X_2). The structure of the metal oxide can be highly diverse depending on the specific environment and continuously changes under different electrochemical conditions.[102] These structural variations contribute significantly to the overall complexity of comprehending the electrochemical interface structure.

The question two: *How does the structure of the solid-liquid interface affect catalytic activity?*

Due to climate change and depleting petroleum supplies, the development of energy conversion technologies, such as fuel cells,[103, 104] water electrolysis,[39, 105] batteries and pseudocapacitors,[7, 58, 63] and CO_2 to fuel conversion,[106, 107] has become increasingly important. The efficiency of these energy conversion systems is largely determined by catalytic processes involving oxygen, namely the oxygen evolution reaction (OER) and the oxygen reduction reaction (ORR), which are known to be sluggish reaction that limit the performance of electrolyzes and fuel cells respectively.[108, 109] Reversibility refers the ability of a chemical reaction to proceed in both the forward and reverse directions under the same conditions. A reversible reaction implies that when the potential is changed in one direction, the reaction

proceeds, and when the potential is reversed, the reaction goes backward. Reversible reactions allow the system to efficiently convert between chemical and electrical energy with minimal losses. Fig. 16 illustrates the half-cell reactions and steady-state polarization curves for the hydrogen evolution reaction (HER) and hydrogen oxidation reaction (HOR) as well as the ORR and OER. It is evident that the catalytic reactions involving oxygen are far more irreversible than hydrogen catalysis, as achieving desirable reaction rates for OER and ORR requires significant overpotentials, even in presence of the best-performing electrocatalysts.[110]

Decades of research on the ORR and OER have not fully elucidated what makes a good catalyst. One significant discovery from computational chemistry community is that the optimal binding strength of oxygen-containing species is crucial for high electrocatalytic performance, aligning with the Sabatier principle, a primary paradigm of heterogeneous catalysis. Rossmeisl, Norskov and others have found that the adsorption energies of these intermediates follow a linear scaling relationship.[111, 112] While computational chemistry provides valuable insights, contradictions often arise between theoretical predictions and electrochemical experiments. Some solid materials with weak oxygen binding energy exhibit excellent oxygen catalysis under specific conditions, while scaling relations would predict low activities.[67, 80, 113] Gold, for instance, known for its inertness, binds oxygen relatively weakly. It indeed demonstrates poor activity for OER and ORR in acidic solutions, yet becomes an excellent catalyst for these reactions in alkaline solutions.[70]

The intricacy of electrocatalytic activity cannot be exclusively attributed to the individual properties of the material, but rather emerges from the combined characteristics of the entire interface environment. This includes the electrode material, the solvent and electrolyte present in the solution, and the structure of the solid-liquid interface. Each of these interactions can affect the electrode surface, thereby exerting a profound influence on the course of the reaction process. Traditional electrochemical theories, like the empirical Butler-Volmer theory, offer limited insights into how the precise solid-liquid interface structure affects the catalytic performance of the electrode in real environments.[108] It is therefore crucial to undertake fundamental investigations to understand how the structure of the solid – liquid interface of catalytic materials influence the catalytic performance. The success of such investigations is

fundamentally rooted in a profound understanding of the interfacial structure, as sought in the first research question. Given the dynamic changes in the catalyst structure during catalytic processes, a genuine representation of the surface structure of the catalyst remains elusive. Similarly, identifying which interactions at the surface-liquid interface hold significance remains a challenge. The existing models, although built upon simple principles predicting scaling relations, are limited in their capacity to elucidate strategies to circumvent these relations. The lack of clear insights into structure - activity correlations underscores the necessity for more comprehensive research, spanning fields such as electrochemistry and materials science, conducted under conditions that mirror real-world scenarios.

Our aim is to gain a profound understanding of the intricate interplay between electrode materials and the complex electrolytic environment within the context of electrocatalytic reactions. This holistic perspective is crucial for uncovering the underlying mechanisms, establishing correlations, and ultimately bridging the knowledge gap that hinders the development of efficient and effective catalytic processes.

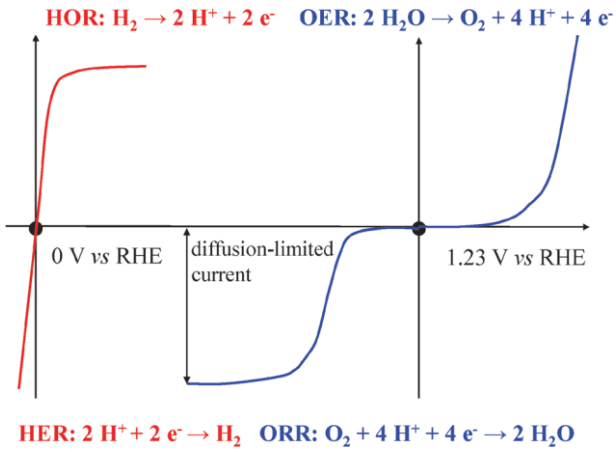

Fig. 16 The polarization curves for two pairs of the key energy-related electrochemical reactions and their overall reaction equations. Red and blue curves refer to the hydrogen-involving and oxygen-involving reactions, respectively. The lines are not drawn to scale. Adapted from Reference [109].

1.6 Structure of the thesis

In this thesis, our attention will be directed towards addressing the two fundamental questions outlined in section 1.5, i.e. *What is the relation between the applied potential and surface charge, and the structure of both the surface and surface-liquid interface?* and *How does the structure of the solid-liquid interface affect catalytic activity?*

To address the two research questions, we conducted an in depth investigation using CV techniques on gold in solutions of varying pH, employing a range of different in situ characterization techniques, such as in situ Surface–Enhanced Raman Spectroscopy (SERS), rotating disk electrode (RDE) techniques, rotating ring-disk electrode (RRDE) techniques, and electrochemical quartz crystal microbalance (EQCM) measurements. Gold, being the noblest metal, is exceptionally well-suited material to carry out such studies and has historically played a pivotal role in pioneering fundamental breakthroughs. Notably, gold's unique properties, including its status as the noblest metal and minimal strength of chemisorption of electrolytes onto its surface, have been well-established.[114-116] These attributes significantly simplify the complexity of the interface structure when using gold as the material of choice.

Our study concentrated on the two core remaining challenges outlined in section 1.5, beginning with a comprehensive investigation into the interface structure within the metal region (X_1) and the oxide region (X_2), respectively. Drawing from the outcomes of these investigations, we formulated various theoretical frameworks to elucidate how the interface structure evolves as a function of various stimuli. Building upon the insights garnered from the first research question regarding the interfacial structure, we were able to comprehend the pH-dependent nature of the oxygen reduction reaction (ORR) and oxygen evolution reaction (OER) activities, as well as the structural alterations accompanying these catalytic processes.

In **Chapter 2**, an in-depth exploration was undertaken to investigate the phenomenon of "peak separation behavior" observed in CVs during gold oxide reduction. The phenomenon involves a scenario where the reduction peak of gold oxide appears singular in an acidic solution, but splits into two peaks in neutral and alkaline solutions. Historically, a conventional model, known as the hydrous oxide model, was utilized to explain this behavior. This model attributed the two reduction peaks to the reduction processes of the inner-monolayer and the outer hydrous layer of the metal oxide surfaces, respectively. Despite its extensive use, the hydrous oxide

model has its limitations, leading to inconsistencies. The central objective of this chapter was to rigorously investigate the inconsistencies intrinsic to the conventional model concerning inner and outer oxide films.

Through rigorous analysis, we initially identified a significant error in the convention hydrous oxide model: On several occasions the a peak that should be attributed to the O_2 reduction reaction on gold was misinterpreted as an oxide reduction peak, particularly in alkaline environments. Additionally, we unveiled the existence of two distinct pH-dependent oxides. The α oxide predominantly manifests in low-pH environments, while the β oxide prevails in high-pH environment. Further study revealed that the two oxides are pivotal for the oxygen evolution reaction (OER) and lead to different OER pathways. This oxide classification was pinpointed by systematic tracing of gold oxide's reduction behavior and conducting in situ surface-enhanced Raman spectroscopy (SERS). This novel discovery of two pH-dependent oxides enabled us to establish a more precise and accurate correlation between the observed reduction peaks and the underlying oxide structures.

By thoroughly exploring the intricacies of the oxide reduction peaks across the entire pH window, we not only challenged the established hydrous oxide model but also revealed the presence of two pH-dependent oxides and their significance in the OER process. The utilization of advanced in situ analytical technique ─ SERS ─ played a crucial role in unraveling the complex oxide structure and forming a deeper understanding of the underlying oxide reduction mechanisms.

In **Chapter 3**, we explored the intriguing "non-Nernstian behavior" characterized by anomalous potential shifts in the oxide reduction peaks of CVs. Although this phenomenon had been noted in various literature reports, it was commonly attributed to solution complexity, with the underlying cause remaining enigmatic. Our study was aimed to uncover the true origin of this behavior.

Our investigation commenced by establishing a direct correlation between the potential shift of the gold oxide reduction peaks and the presence of Au^{3+} cations within oxide layer. Remarkably, this discovery not only unveiled the underlying mechanism for variations in oxide

structure across different solution environments but also elucidated why the oxide structure evolves during catalytic processes. The crucial factor lies in binding of formed Au^{3+} cations to the gold oxide.

Our exploration was facilitated by employing advanced in situ techniques, including RRDE and EQCM. These tools enabled us to probe deeply into the intricacies of the amorphous oxide structure within realistic catalytic environments. This pivotal discovery not only demystified the elusive nature of the amorphous oxide structure but also offered a dynamic perspective, providing insight into the evolving oxide structure. Furthermore, our findings highlighted the interface changes driven by electrostatic interactions involving surface gold cations, influencing the complex oxygen evolution reaction at the dynamic oxide interface.

The adept application of sophisticated methodologies like RRDE and EQCM allowed us to unravel intricacies that were previously obscured, fostering a more clear understanding of the intricate interplay among oxide structures, electrostatic interactions, and catalytic reactions at the oxide interface.

In **Chapter 4**, our focus was dedicated to unraveling the intricate current response behaviors within the electrochemical double layer region. This current encompasses both Faradaic current, involving electron transfer, and non-Faradaic current, arising from electrostatic interactions. For an extended duration, accurately identifying and quantifying these two currents has posed limitations on our understanding of the surface charge, a factor that directly influences the strength of the interfacial electric field.

Our investigation was centered on deciphering the connection between the current response in cyclic voltammetry (CV) and the frequency response observed by quartz crystal microbalance (QCM) measurements. A primary objective was to establish a quantitative framework for determination of the surface charge, even in the presence of complexities introduced by chemisorption and even the electrocatalytic oxygen reduction process.

Through our research, we devised a direct in situ method for both identifying and quantifying the surface charge. This innovative approach marked a significant advancement in our ability to unravel the interplay between the surface charges and the chemistry occurring at

the interface. Moreover, this method enabled us to directly observe the dynamic changes in the surface charge during the catalytic oxygen reduction reaction (ORR).

By systematically investigating the current response, we have not only enriched our understanding of the dynamics within the electrochemical double layer but also developed a potent toolkit for assessing surface charge variations across diverse electrochemical conditions. This achievement offers a novel perspective to examine the relation between the surface charge and the interface structure on gold, paving the way for more nuanced insights into catalytic reactions, such as ORR, and their underlying mechanisms.

Throughout this thesis, a series of foundational insights regarding electrochemical signals have been uncovered through discovered by a comprehensive integration of detailed CV behavior investigations and various in situ techniques applied to gold electrodes. These newfound insights provide a fresh standpoint, simplifying the comprehension of complex interface environments.

References

1. Reinmuth, W. H., *Analytical Chemistry* **1960,** *32* (11), 1509-1512.
2. Bard, A. K.; Zoski, C. G., *Analytical Chemistry* **2000,** *72* (9), 346A-352A.
3. Budnikov, G. K.; Shirokova, V. I., *Journal of Analytical Chemistry* **2009,** *64* (12), 1279-1288.
4. Augustyn, V.; Simon, P.; Dunn, B., *Energy & Environmental Science* **2014,** *7* (5).
5. Elgrishi, N.; Rountree, K. J.; McCarthy, B. D.; Rountree, E. S.; Eisenhart, T. T.; Dempsey, J. L., *Journal of Chemical Education* **2018,** *95* (2), 197-206.
6. Rountree, E. S.; McCarthy, B. D.; Eisenhart, T. T.; Dempsey, J. L., *Inorg Chem* **2014,** *53* (19), 9983-10002.
7. Simon, P.; Gogotsi, Y.; Dunn, B., *Science* **2014,** *343* (6176), 1210-1211.
8. Brousse, T.; Bélanger, D.; Long, J. W., *Journal of The Electrochemical Society* **2015,** *162* (5), A5185-A5189.
9. Pu, X.; Zhao, D.; Fu, C.; Chen, Z.; Cao, S.; Wang, C.; Cao, Y., *Angew Chem Int Ed Engl* **2021,** *60* (39), 21310-21318.
10. Macdonald, D. D.; Qiu, J., *Journal of Solid State Electrochemistry* **2020,** *24* (11-12), 2663-2677.
11. Mansfeld, F., *Journal of Solid State Electrochemistry* **2008,** *13* (4), 515-520.
12. Conway, B. E., *Prog. Surf. Sci.* **1995,** *49* (4), 331-452.
13. Diaz-Cruz, J. M.; Serrano, N.; Perez-Rafols, C.; Arino, C.; Esteban, M., *J Solid State Electrochem* **2020,** *24* (11-12), 2653-2661.
14. Lubert, K.-H.; Kalcher, K., *Electroanalysis* **2010,** *22* (17-18), 1937-1946.
15. Guin, S. K.; Ambolikar, A. S.; Das, S.; Poswal, A. K., *Electroanalysis* **2020,** *32* (7), 1629-1641.
16. Nong, H. N.; Falling, L. J.; Bergmann, A.; Klingenhof, M.; Tran, H. P.; Spori, C.; Mom, R.; Timoshenko, J.; Zichittella, G.; Knop-Gericke, A.; Piccinin, S.; Perez-Ramirez, J.; Cuenya, B. R.; Schlogl, R.; Strasser, P.; Teschner, D.; Jones, T. E., *Nature* **2020,** *587* (7834), 408-413.
17. Kolb, D. M., *Prog. Surf. Sci.* **1996,** *51* (2), 109-173.
18. Sarma, A. K.; Vatsyayan, P.; Goswami, P.; Minteer, S. D., *Biosens Bioelectron* **2009,** *24* (8), 2313-22.
19. Heyrovský, M., *Journal of Solid State Electrochemistry* **2010,** *15* (7-8), 1799-1803.
20. Bard, A. J., *Journal of Chemical Education* **2007,** *84* (4), 644.
21. Smutok, O.; Katz, E., *Journal of Solid State Electrochemistry* **2023**.
22. Hájková, A.; Vyskočil, V.; Barek, J.; Němcová, V. In *The current role of polarography in the light of the coming 90th anniversary of its discovery (a reflection)*, 2011.
23. Heyrovský, M., Catalytic Hydrogen Evolution at Mercury Electrodes from Solutions of Peptides and Proteins. In *Perspectives in Bioanalysis*, Paleček, E.; Scheller, F.; Wang, J., Eds. Elsevier: 2005; Vol. 1, pp 657-687.
24. Barek, J.; Zima, J., *Electroanalysis* **2003,** *15* (5-6), 467-472.
25. Senturk, Z., *Crit Rev Anal Chem* **2022**, 1-12.
26. Heyrovský, J.; Shikata, M., *Recueil des Travaux Chimiques des Pays-Bas* **1925,** *44* (6), 496-498.
27. Kolthoff, I. M.; Laitinen, H. A., *Science* **1940,** *92* (2381), 152-154.
28. Scholz, F., *Journal of Solid State Electrochemistry* **2010,** *15* (7-8), 1509-1521.
29. Colburn, A. W.; Levey, K. J.; O'Hare, D.; Macpherson, J. V., *Phys Chem Chem Phys* **2021,** *23* (14), 8100-8117.
30. Kolotyrkin, Y. M.; Losev, V. V.; Chemodanov, A. N., *Materials Chemistry and Physics* **1988,** *19* (1), 1-95.
31. Yi, Y.; Weinberg, G.; Prenzel, M.; Greiner, M.; Heumann, S.; Becker, S.; Schlögl, R., *Catalysis Today* **2017,** *295*, 32-40.
32. Grdeń, M.; Łukaszewski, M.; Jerkiewicz, G.; Czerwiński, A., *Electrochim. Acta* **2008,** *53* (26), 7583-7598.
33. Cherevko, S.; Topalov, A. A.; Zeradjanin, A. R.; Katsounaros, I.; Mayrhofer, K. J. J., *RSC Adv.* **2013,** *3* (37).
34. Luo, M.; Koper, M. T. M., *Nat. Catal.* **2022,** *5* (7), 615-623.
35. Chen, X.; McCrum, I. T.; Schwarz, K. A.; Janik, M. J.; Koper, M. T. M., *Angew Chem Int Ed Engl* **2017,** *56* (47), 15025-15029.
36. Gorlin, M.; Ferreira de Araujo, J.; Schmies, H.; Bernsmeier, D.; Dresp, S.; Gliech, M.; Jusys, Z.; Chernev, P.; Kraehnert, R.; Dau, H.; Strasser, P., *J Am Chem Soc* **2017,** *139* (5), 2070-2082.
37. Gorlin, M.; Halldin Stenlid, J.; Koroidov, S.; Wang, H. Y.; Borner, M.; Shipilin, M.; Kalinko, A.; Murzin, V.; Safonova, O. V.; Nachtegaal, M.; Uheida, A.; Dutta, J.; Bauer, M.; Nilsson, A.; Diaz-Morales, O., *Nat Commun* **2020,** *11* (1), 6181.
38. Trzesniewski, B. J.; Diaz-Morales, O.; Vermaas, D. A.; Longo, A.; Bras, W.; Koper, M. T.; Smith, W. A., *J. Am. Chem. Soc.* **2015,** *137* (48), 15112-21.
39. Costentin, C.; Dridi, H.; Saveant, J. M., *J Am Chem Soc* **2015,** *137* (42), 13535-44.
40. Langerman, M.; Hetterscheid, D. G. H., *Angew Chem Int Ed Engl* **2019,** *58* (37), 12974-12978.
41. Laurence D. Burke, L. D. B., Electrochemistry of hydrous oxide films. *Modern Aspects of Electrochemistry* 1986 pp 169-189.
42. Miller, F. J.; Zittel, H. E., *Analytical Chemistry* **1963,** *35* (12), 1866-&.

43. Zittel, H. E.; Miller, F. J., *Analytical Chemistry* **1965,** *37* (2), 200-&.
44. Yoshimori, T.; Arakawa, M.; Takeuchi, T., *Talanta* **1965,** *12* (2), 147-152.
45. Tonelli, D.; Scavetta, E.; Giorgetti, M., *Anal Bioanal Chem* **2013,** *405* (2-3), 603-14.
46. Walcarius, A., *Chemistry of Materials* **2001,** *13* (10), 3351-3372.
47. Alves, W. A.; Matos, I. O.; Takahashi, P. M.; Bastos, E. L.; Martinho, H.; Ferreira, J. G.; Silva, C. C.; de Almeida Santos, R. H.; Paduan-Filho, A.; Da Costa Ferreira, A. M., *European Journal of Inorganic Chemistry* **2009,** *2009* (15), 2219-2228.
48. Royzen, M.; Wilson, J. J.; Lippard, S. J., *J Inorg Biochem* **2013,** *118*, 162-70.
49. Eftekhari, A., *Journal of Power Sources* **2017,** *343*, 395-411.
50. Goodridge, F.; King, C. J. H.; Wright, A. R., *Electrochim. Acta* **1977,** *22* (4), 347-352.
51. Karlsson, R. K.; Cornell, A., *Chem Rev* **2016,** *116* (5), 2982-3028.
52. Trasatti, S., *Electrochim. Acta* **2000,** *45* (15), 2377-2385.
53. McHenry, E. J., *Electrochemical Technology* **1967,** *5* (5-6), 275-&.
54. Ikeda, H.; Saito, T.; Tamura, H., *Cleveland Section of the Electrochemical Society* **1975**, 384.
55. Tarascon, J. M.; Armand, M., *Nature* **2001,** *414* (6861), 359-367.
56. Steele, B., *Ed. W. van Gool, North Holland, Amsterdam* **1973**, 103.
57. Van Gool, W., **1973**.
58. Fleischmann, S.; Mitchell, J. B.; Wang, R.; Zhan, C.; Jiang, D.-e.; Presser, V.; Augustyn, V., *Chemical Reviews* **2020,** *120* (14), 6738-6782.
59. Scholz, F.; Leiva, E. P. M., *ChemElectroChem* **2018,** *5* (6), 849-854.
60. Trasatti, S.; Buzzanca, G., *Journal of Electroanalytical Chemistry and Interfacial Electrochemistry* **1971,** *29* (2), A1-A5.
61. Lu-Lu Zhang, C.-K. L., Jun Huang, *Journal of Electrochemistry* **2022,** *28* (2), 2108471.
62. Boettcher, S. W.; Oener, S. Z.; Lonergan, M. C.; Surendranath, Y.; Ardo, S.; Brozek, C.; Kempler, P. A., *ACS Energy Letters* **2020,** *6* (1), 261-266.
63. Noori, A.; El-Kady, M. F.; Rahmanifar, M. S.; Kaner, R. B.; Mousavi, M. F., *Chem Soc Rev* **2019,** *48* (5), 1272-1341.
64. Costentin, C.; Porter, T. R.; Saveant, J. M., *ACS Appl Mater Interfaces* **2017,** *9* (10), 8649-8658.
65. Yang, X.; Rogach, A. L., *Advanced Energy Materials* **2019,** *9* (25).
66. Simon, P.; Gogotsi, Y., *Nature Materials* **2008,** *7* (11), 845-854.
67. Ramaswamy, N.; Mukerjee, S., *The Journal of Physical Chemistry C* **2011,** *115* (36), 18015-18026.
68. Viswanathan, V.; Hansen, H. A.; Rossmeisl, J.; Norskov, J. K., *J Phys Chem Lett* **2012,** *3* (20), 2948-51.
69. Strobl, J. R.; Scherson, D., *The Journal of Physical Chemistry C* **2021,** *125* (25), 13862-13870.
70. Ramaswamy, N.; Mukerjee, S., *Advances in Physical Chemistry* **2012,** *2012*, 1-17.
71. Vesztergom, S.; Ujvári, M.; Láng, G. G., *Electrochem. commun.* **2011,** *13* (4), 378-381.
72. Dalton, F., *Electrochemical Society Interface* **2016,** *25* (3), 50-59.
73. Yang, S.; Hetterscheid, D. G. H., *ACS Catal.* **2020,** *10* (21), 12582-12589.
74. Jin, L.; Seifitokaldani, A., *Catalysts* **2020,** *10* (5), 481.
75. Wahab, O. J.; Kang, M.; Unwin, P. R., *Current Opinion in Electrochemistry* **2020,** *22*, 120-128.
76. Kautek, W.; Sahre, M.; Soares, D. M., *Ber. Bunsenges. Phys. Chem.* **1995,** *99* (4), 667-676.
77. Tsai, W. Y.; Taberna, P. L.; Simon, P., *J Am Chem Soc* **2014,** *136* (24), 8722-8.
78. Patel, A. N.; Collignon, M. G.; O'Connell, M. A.; Hung, W. O.; McKelvey, K.; Macpherson, J. V.; Unwin, P. R., *J Am Chem Soc* **2012,** *134* (49), 20117-30.
79. Mei, D.; He, Z. D.; Zheng, Y. L.; Jiang, D. C.; Chen, Y. X., *Phys Chem Chem Phys* **2014,** *16* (27), 13762-73.
80. Prieto, A.; Hern**&#65533;**ndez, J.; Herrero, E.; Feliu, J. M., *Journal of Solid State Electrochemistry* **2003,** *7* (9), 599-606.
81. Escudero-Escribano, M.; Jensen, K. D.; Jensen, A. W., *Current Opinion in Electrochemistry* **2018,** *8*, 135-146.
82. Sauerbrey, G., *Zeitschrift Fur Physik* **1959,** *155* (2), 206-222.
83. Horst, R. J.; Katzourakis, A.; Mei, B. T.; de Beer, S., *HardwareX* **2022,** *12*, e00374.
84. Buttry, D. A.; Ward, M. D., *Chemical Reviews* **1992,** *92* (6), 1355-1379.
85. Schley, N. D.; Blakemore, J. D.; Subbaiyan, N. K.; Incarvito, C. D.; D'Souza, F.; Crabtree, R. H.; Brudvig, G. W., *J Am Chem Soc* **2011,** *133* (27), 10473-81.
86. Hetterscheid, D. G. H., *Chem Commun (Camb)* **2017,** *53* (77), 10622-10631.
87. Hillman, A. R., *Journal of Solid State Electrochemistry* **2011,** *15* (7-8), 1647-1660.
88. Gordon, J. S.; Johnson, D. C., *Journal of Electroanalytical Chemistry* **1994,** *365* (1), 267-274.
89. Hubkowska, K.; Łukaszewski, M.; Czerwiński, A., Quartz crystal nanobalance measurements in electrocatalysis. In *Encyclopedia of Interfacial Chemistry*, Wandelt, K., Ed. Elsevier: Oxford, 2018; pp 402-412.
90. Le, J.; Iannuzzi, M.; Cuesta, A.; Cheng, J., *Phys Rev Lett* **2017,** *119* (1), 016801.
91. Frumkin, A. N.; Petrii, O. A., *Electrochim. Acta* **1975,** *20* (5), 347-359.
92. Chen, J.; Nie, L.; Yao, S., *Journal of Electroanalytical Chemistry* **1996,** *414* (1), 53-59.

93. Payne, R., Double Layer at the Mercury-Solution Interface. In *Progress in Surface and Membrane Science*, Danielli, J. F.; Rosenberg, M. D.; Cadenhead, D. A., Eds. Elsevier: 1973; Vol. 6, pp 51-123.
94. Hamann, C. H.; Hamnett, A.; Vielstich, W., *Electrochemistry*. 2nd completely rev. and updated ed. ed.; Weinheim : Wiley: 2007.
95. Schmickler, W., *Chemical Reviews* **1996,** *96* (8), 3177-3200.
96. Jeanmairet, G.; Rotenberg, B.; Salanne, M., *Chem Rev* **2022,** *122* (12), 10860-10898.
97. Xiao, Y.; Xu, R.; Yan, C.; Huang, J. Q.; Zhang, Q.; Ouyang, M., *Advanced Functional Materials* **2021,** *32* (13).
98. Bard, A. J.; Inzelt, G.; Scholz, F., *Electrochemical dictionary*. Springer: 2012.
99. Song, J.; Wei, C.; Huang, Z. F.; Liu, C.; Zeng, L.; Wang, X.; Xu, Z. J., *Chem. Soc. Rev.* **2020,** *49* (7), 2196-2214.
100. Huang, J., *JACS Au* **2023,** *3* (2), 550-564.
101. Cherevko, S.; Zeradjanin, A. R.; Keeley, G. P.; Mayrhofer, K. J. J., *Journal of The Electrochemical Society* **2014,** *161* (12), H822-H830.
102. Ding, H.; Liu, H.; Chu, W.; Wu, C.; Xie, Y., *Chem. Rev.* **2021,** *121* (21), 13174-13212.
103. Yuan, C.; Wu, H. B.; Xie, Y.; Lou, X. W., *Angew. Chem. Int. Ed. Engl.* **2014,** *53* (6), 1488-504.
104. Stamenkovic, V. R.; Strmcnik, D.; Lopes, P. P.; Markovic, N. M., *Nat Mater* **2016,** *16* (1), 57-69.
105. Chen, X.; Aschaffenburg, D. J.; Cuk, T., *Nat. Catal.* **2019,** *2* (9), 820-827.
106. Deng, B.; Huang, M.; Zhao, X.; Mou, S.; Dong, F., *ACS Catalysis* **2021,** *12* (1), 331-362.
107. Dunwell, M.; Luc, W.; Yan, Y.; Jiao, F.; Xu, B., *ACS Catalysis* **2018,** *8* (9), 8121-8129.
108. Koper, M. T. M., *Chem. Sci.* **2013,** *4* (7), 2710-2723.
109. Jiao, Y.; Zheng, Y.; Jaroniec, M.; Qiao, S. Z., *Chem Soc Rev* **2015,** *44* (8), 2060-86.
110. Zeradjanin, A. R., *Current Opinion in Electrochemistry* **2018,** *9*, 214-223.
111. Man, I. C.; Su, H. Y.; Calle-Vallejo, F.; Hansen, H. A.; Martínez, J. I.; Inoglu, N. G.; Kitchin, J.; Jaramillo, T. F.; Nørskov, J. K.; Rossmeisl, J., *ChemCatChem* **2011,** *3* (7), 1159-1165.
112. Rossmeisl, J.; Logadottir, A.; Nørskov, J. K., *Chemical Physics* **2005,** *319* (1-3), 178-184.
113. Blizanac, B. B.; Ross, P. N.; Markovic, N. M., *Electrochim. Acta* **2007,** *52* (6), 2264-2271.
114. Peuckert, M.; Coenen, F. P.; Bonzel, H. P., *Surf. Sci.* **1984,** *141* (2-3), 515-532.
115. Burke, L. D.; Nugent, P. F., *Gold Bull.* **1997,** *30* (2), 43-53.
116. Weiher, N.; Willneff, E. A.; Figulla-Kroschel, C.; Jansen, M.; Schroeder, S. L. M., *Solid State Commun.* **2003,** *125* (6), 317-322.